# Automatic Adaptive Control of Friction Stir Welding

Kevin Colligan and Johnathon Hunt
Concurrent Technologies Corporation (CTC)
Johnstown, PA USA

Ryan Tedjasukmana and Daniel Langan
PAR Systems
Shoreview, MN USA

## Abstract

Production friction stir welding often relies on fixed parameters that fail when boundary conditions vary. This paper presents an adaptive control method that modulates machine settings in real-time using spindle torque data to maintain constant flow stress and energy density. Validated on 12.7-mm 7075-T651 aluminum, the system ensured volumetric integrity across extreme thermal variations and reduced mechanical distortion. However, microhardness results indicate that constant energy density is insufficient to preserve properties in restricted boundaries due to reduced cooling rates, which led to a 96 Hv hardness plateau. These findings suggest that while adaptive control ensures weld soundness, additional strategies like variable weld pitch or active cooling are necessary to manage the properties of quench-sensitive alloys.

## Introduction

Friction stir welding (FSW) is uniquely sensitive to thermal conduction boundary conditions compared to traditional arc welding. In production, complex structural geometries often create variable heat dissipation paths that can degrade weld formation if machine settings remain fixed. While pre-programmed parameter changes can mitigate these effects, this approach is costly, time-consuming, and fails to account for unplanned variability, such as inconsistent workpiece-to-fixture fit-up. These challenges necessitate an adaptive control system capable of responding to real-time thermal changes to ensure stable joint quality through automated adjustment.

Temperature control has been demonstrated as an effective means of adaptively modifying machine settings to maintain constant tool temperature in FSW [1-6]. These studies showed that maintaining a constant temperature can automatically prevent volumetric defects despite significant variations in boundary conditions. Presumably, this stability also maintains constant conditions within the stir zone, thereby ensuring consistent joint properties. The experiments reported here were designed to test this hypothesis.

Prior work has established that spindle torque reflects peak weld zone temperature and serves as a reliable predictor of volumetric soundness [7-11]. Specifically, "unit-area analysis" was developed to normalize process conditions across varying tool sizes and workpiece thicknesses. These studies demonstrated that maintaining a constant average flow stress, calculated from torque and tool geometry, optimizes quality in 7075-T651 aluminum. While this principle was previously validated through manual adjustments of spindle and welding speeds, such methods lacked precision. The present paper describes


DISTRIBUTION STATEMENT A. Approved for public release; distribution is unlimited. OPSEC#10639

the implementation and results of a fully automated system for controlling spindle torque and weld pitch on a PAR Systems (Shoreview, MN, USA) welding machine.

## Background

The present work addresses the automatic control of machine settings to maintain constant spindle torque despite variable boundary conditions. Preliminary, manual testing demonstrated that while both spindle and welding speeds could control torque, spindle speed was the more responsive variable. However, experimental observations indicated that manipulating spindle speed alone altered the weld pitch, defined as the ratio of welding speed to spindle speed. As spindle speed was reduced in response to constricted boundary conditions, the resulting increase in pitch threatened to exceed the tool's capacity to maintain joint soundness. Consequently, a constant weld pitch requirement was integrated into the control algorithm to prevent volumetric defect formation.

Maintaining constant weld pitch alongside spindle torque offers a theoretical pathway to constant energy density ($\rho_E$), which correlates to joint transverse tensile strength under steady-state boundary conditions [7]. Energy density is calculated as:

$$\rho_E = \frac{2\pi T}{weld\ pitch \times total\ tool\ area} \tag{1}$$

where $T$ is the spindle torque and total tool area represents the tool-workpiece interface. This relationship implies that if torque is stabilized by modulating spindle speed, and weld pitch is maintained through proportional adjustments to welding speed, the energy density remains constant. While boundary conditions often fluctuate in practice, this dual-variable approach prevents "pitch capacity" defects while potentially mitigating the degradation of tensile properties.

Manual testing demonstrated that maintaining constant spindle torque allowed the tool to traverse constricted boundary conditions while under constant plunge force, which was initially set in a region with high heat-sink capacity. This result was surprising, as welding in load control typically fails when transitioning to restricted boundaries under fixed machine settings. In those cases, decreased heat conduction leads to higher temperatures in the weld zone, causing the tool to plunge deeper and produce excess flash. However, by modulating spindle speed to stabilize torque, with torque as a proxy for weld zone temperature, it became possible to maintain load control independent of changing boundary conditions.

Based on these observations, an algorithm was developed for the adaptive control of flow stress and weld pitch, shown in Figure 1. Input parameters include setpoints for spindle torque (equivalent to flow stress), plunge force (equivalent to shoulder pressure), and weld pitch, along with spindle and welding speed limits to respect machine constraints. During each control loop, the system compares the measured spindle torque against the setpoint and modulates the spindle speed to reduce the error. Every adjustment to spindle speed triggers a proportional change in welding speed to maintain the commanded weld pitch. This algorithm was validated through manual adjustments at CTC (Concurrent Technologies Corporation) and via fully automated control at PAR Systems.


DISTRIBUTION STATEMENT A. Approved for public release; distribution is unlimited. OPSEC#10639

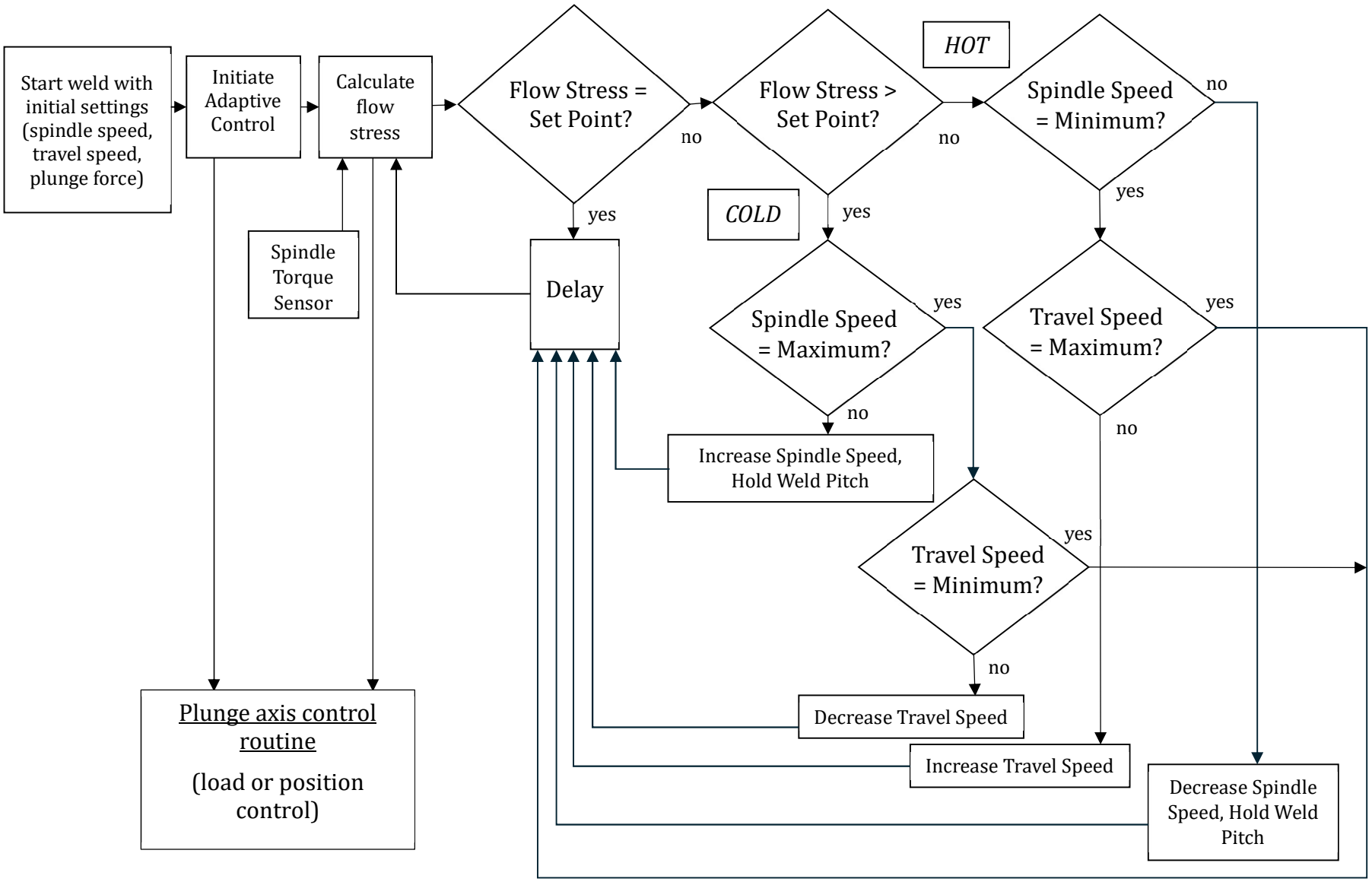


Figure 1. Flow Stress Control with Pitch Control algorithm.


DISTRIBUTION STATEMENT A. Approved for public release; distribution is unlimited. OPSEC#10639

## Experimental Approach

The performance of automated flow stress control, both with and without simultaneous weld pitch regulation, was evaluated at PAR Systems. All welds utilized 12.7-mm 7075-T651 aluminum plates. The welding tool featured a 30.5-mm diameter flat, scrolled shoulder and a threaded, frustum-shaped pin with four flats (12.5-mm root and 9.5-mm tip diameters) [7]. To evaluate the controller's response, three boundary conditions were tested. Baseline bead-on-plate welds were performed on 305-mm by 1,220-mm plates with uniform thermal conditions. Variable boundary conditions were then introduced by machining slots parallel to the weld path (Figure 2 and Figure 3). To further alter thermal conduction, some slots featured close-fitting steel bars. The test panel design allowed three experimental runs per plate.

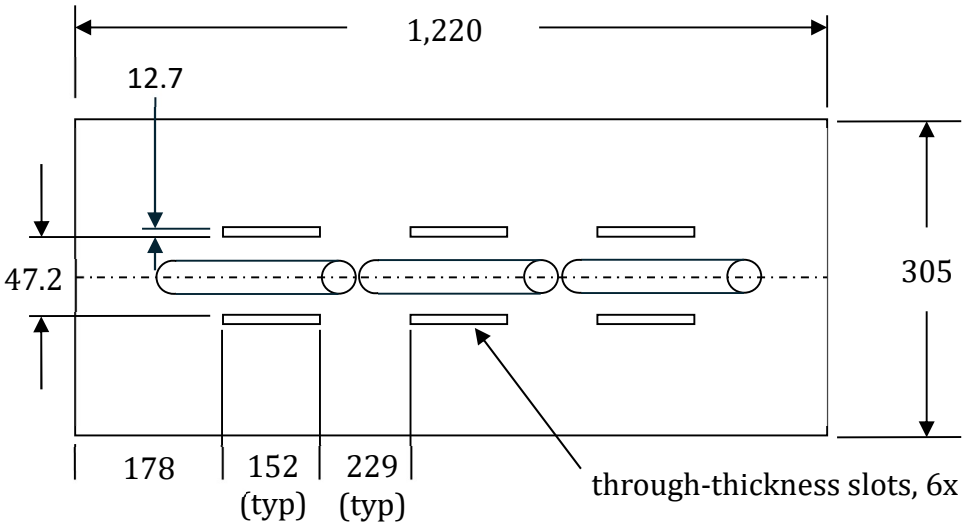


Figure 2. "Slotted" test panel for testing automated weld control with variable boundary conditions. All dimensions in millimeters.

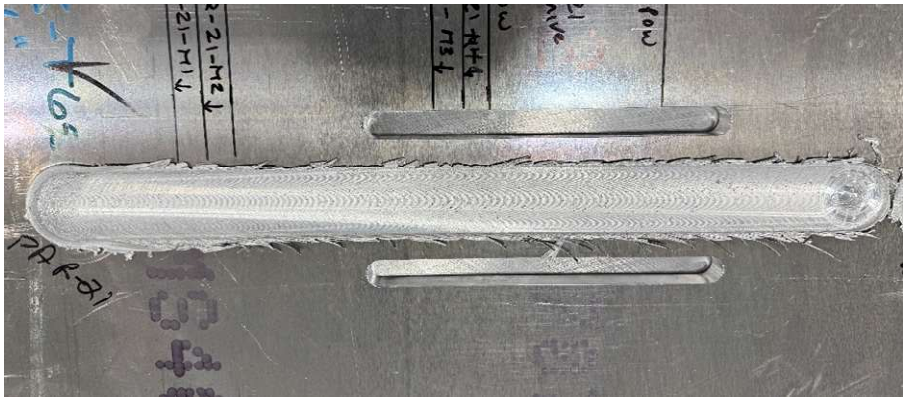

Figure 3. Overview of weld PAR-21.

The experimental runs are summarized in Table 1. Two sets of welds were performed, each representing a distinct flow stress setpoint. The "hot" set targeted a flow stress of approximately 30 MPa. Prior experiments at CTC indicated this value would produce sound


DISTRIBUTION STATEMENT A. Approved for public release; distribution is unlimited. OPSEC#10639

welds while remaining near the lower threshold for high-temperature weld quality [7]. The "moderate" set utilized a 42 MPa setpoint, representing a lower peak temperature intended to ensure volumetric soundness. Both sets included a baseline run on a solid plate (identified as PAR-14 and PAR-12 in Table 1) to establish steady-state conditions under automated flow stress control.

Table 1. Welds performed during welding control algorithm tests at PAR Systems.

| Weld ID | Axial Control | Torque Control | Pitch Control | Section Description | Key or No Key | Spindle Speed | Welding Speed | Pitch | Flow Stress (setpoint) | Flow Stress (measured) | Energy Density |
|---|---|---|---|---|---|---|---|---|---|---|---|
| | | | | | | rev/min | mm/s | mm/rev | MPa | MPa | J/mm^3 |
| PAR-1-M1 | Position | | | Wide | n/a | 283.0 | 1.58 | 0.34 | n/a | 23.3 | 2.04 |
| PAR-1-M2 | Position | | | Slotted | No Key | 305.5 | 1.57 | 0.31 | n/a | 14.8 | 1.40 |
| | | | | | | | | | | | |
| PAR-14 | Load | yes | yes | Wide | n/a | 190.3 | 1.48 | 0.47 | 30.25 | 30.2 | 2.03 |
| PAR-9 | Load | yes | | Slotted | No Key | 161.8 | 1.48 | 0.55 | 30.16 | 30.1 | 1.72 |
| PAR-17 | Load | yes | yes | Slotted | No Key | 151.7 | 1.16 | 0.46 | 30.25 | 30.3 | 2.08 |
| PAR-21 | Load | yes | yes | Slotted | Key | 171.5 | 1.30 | 0.46 | 30.09 | 30.0 | 2.06 |
| | | | | | | | | | | | |
| PAR-12 | Load | yes | | Wide | n/a | 148 | 2.12 | 0.86 | 41.98 | 41.8 | 1.52 |
| PAR-22 | Load | yes | yes | Slotted | Key | 138 | 1.98 | 0.86 | 41.88 | 41.8 | 1.52 |

All welds were performed on a PAR Systems PDS welding system. A typical run commenced by plunging the tool to the target depth, followed by a 50-mm travel segment under conventional, fixed-parameter control. Upon completing this startup phase, the system automatically engaged either flow stress control alone or in conjunction with weld pitch control, as dictated by the experimental plan. In this mode, the controller modulated spindle and travel speeds to maintain the established setpoints. Prior to weld termination, the algorithm was disengaged, and the system returned to fixed machine settings for the final segment.

## Results

Data from weld PAR-1 (Figure 4), illustrates the impact of variable boundary conditions under fixed machine settings. In the wide section of the plate, the weld exhibited a baseline flow stress of approximately 23 MPa. Upon encountering the slotted section at 140 mm, the flow stress dropped to a minimum of 15.5 MPa at the 210-mm mark. A manual increase in spindle speed from 210 to 290 rev/min further reduced the flow stress to a minimum of 13.7 MPa. After the tool exited the slotted section and heat-sink capacity increased, the flow stress recovered to approximately 20 MPa by the end of the weld.


DISTRIBUTION STATEMENT A. Approved for public release; distribution is unlimited. OPSEC#10639

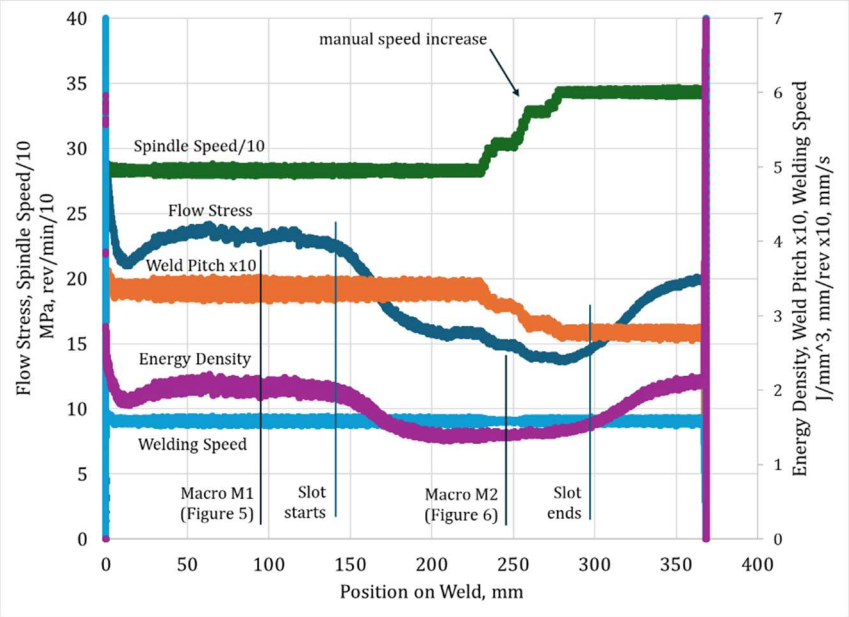


Figure 4. Data from weld PAR-1, made with manually controlled machine settings.

The macro section from specimen PAR-1-M1, taken from 89 mm into the weld while the welding tool was in the wide section of plate, is shown in Figure 5 with the welding tool profile overlaid on the image. The macro section reveals pronounced upward distortion of the prior grain structure in the thermo-mechanically affected zone (TMAZ) on both the advancing and retreating sides. No volumetric defects were observed. In this portion of the weld, the energy density reached approximately 2.04 J/mm$^3$. The high energy density implies an elevated temperature distribution, leading to elevated thermal softening which may have resulted in the large distortion of the prior grain structure in the TMAZ.

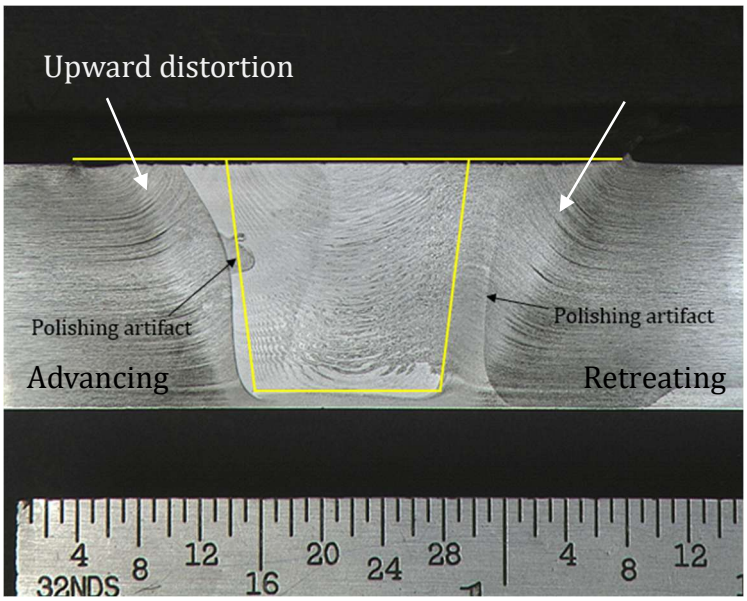


Figure 5. Macro section PAR-1-M1 with the welding tool profile overlaid, scale is in inches.


DISTRIBUTION STATEMENT A. Approved for public release; distribution is unlimited. OPSEC#10639

The macro section for specimen PAR-1-M2 is shown in Figure 6. In this section of the weld, the flow stress dropped to 14.8 MPa, a result of the restricted boundary condition exacerbated by the higher spindle speed compared to section M1. Previous experiments in this program indicated that flow stress values below 30 MPa significantly increase the probability of internal defects and other quality demerits in 7075-T651 aluminum. This specific sample confirms that risk, exhibiting cavity defects [7]. The goal of using flow stress control is to automatically adjust the machine settings to avoid this large drop in flow stress and thereby prevent the formation of this type of volumetric defect.

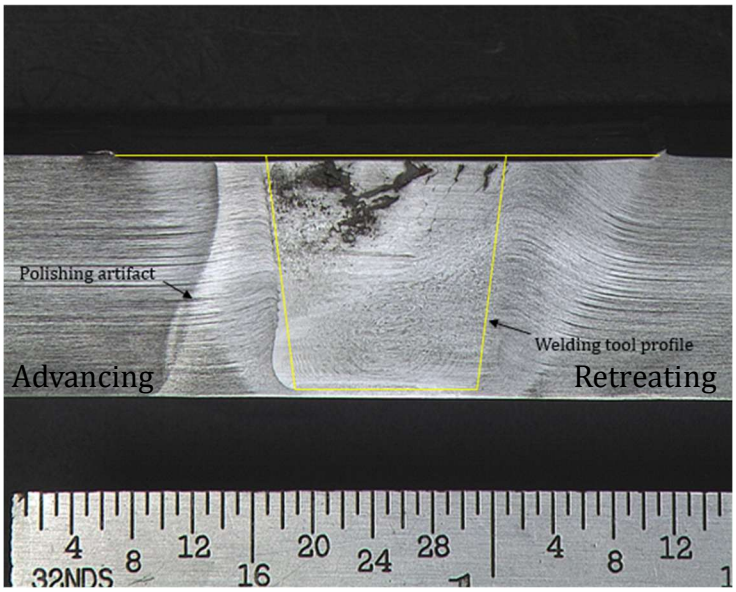


Figure 6. Macro section PAR-1-M2, with the welding tool profile overlaid.

Figure 7 displays the data for weld PAR-21, a representative run under simultaneous flow stress and weld pitch control. The process began at 191 rev/min and 1.27 mm/s with a plunge force of 38.7 kN. After 50 mm of travel, the system engaged automated control, targeting a flow stress of 30.09 MPa and a pitch of 0.46 mm/rev. Following a brief initial stabilization, the controller responded to the slotted section by reducing the spindle speed to maintain the flow stress setpoint. The pitch control loop then triggered a proportional reduction in welding speed. Upon exiting the restricted boundary, the controller increased both speeds, returning to near-baseline settings before disengaging near the weld's end. Notably, because spindle torque remained constant, the heat flux (power per unit area) tracked the spindle speed adjustments, reflecting the reduced power required to maintain torque within the constricted thermal boundary.


DISTRIBUTION STATEMENT A. Approved for public release; distribution is unlimited. OPSEC#10639

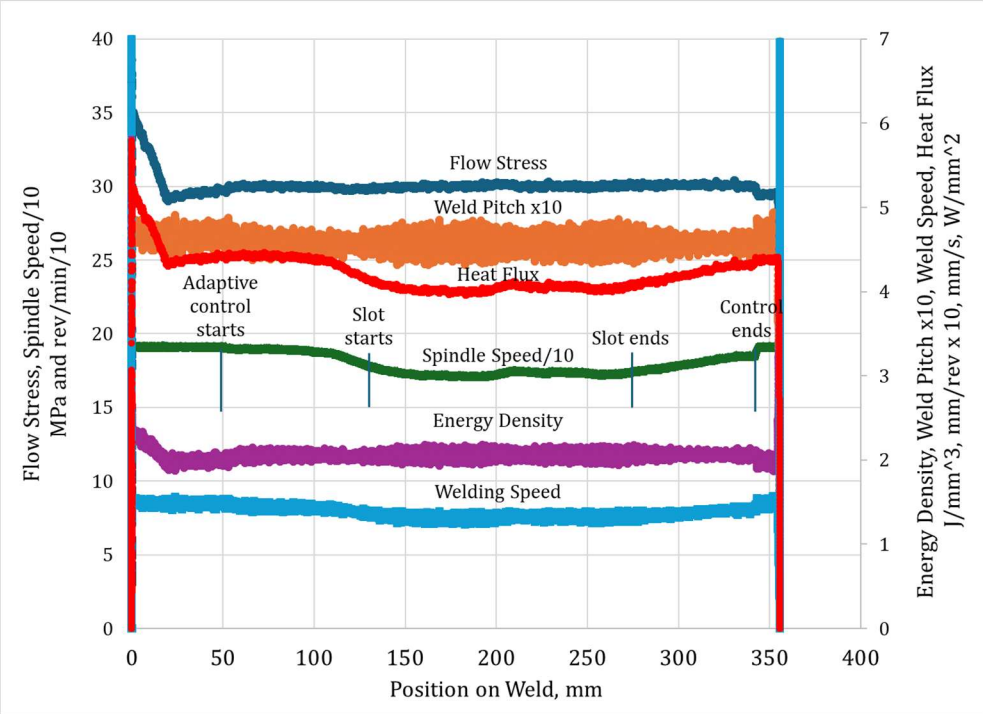


Figure 7. Data from a typical weld made in combined flow stress and pitch control mode, weld PAR-21.

Welds were evaluated through log file analysis, visual crown inspection, transverse macro-sections, and microhardness testing. Because the reduced width of the slotted sections precluded standard transverse tensile testing, microhardness profiles served as the primary indicator of local thermal cycles and mechanical strength. This approach provided high-resolution insight into the property variations across the weld zones (nugget, TMAZ, and heat-affected zone (HAZ)). Additionally, phased-array ultrasonic testing (PAUT) confirmed that all automated runs were free of internal defects.

Figure 8 shows a typical macro section from the slotted region of weld PAR-17, which is free of volumetric defects. Notably, the upward distortion of the prior grain structure in the TMAZ is significantly less pronounced than in specimens PAR-1-M1 and PAR-1-M2. This may be explained by the lower lateral force, defined here as the vector sum of longitudinal and transverse forces, recorded for PAR-17. The force dropped from 7.6 kN (PAR-1-M1) and 8.2 kN (PAR-1-M2) to 5.2 kN in PAR-17. This indicates that reducing the mechanical force can directly reduce grain distortion in the TMAZ.


DISTRIBUTION STATEMENT A. Approved for public release; distribution is unlimited. OPSEC#10639

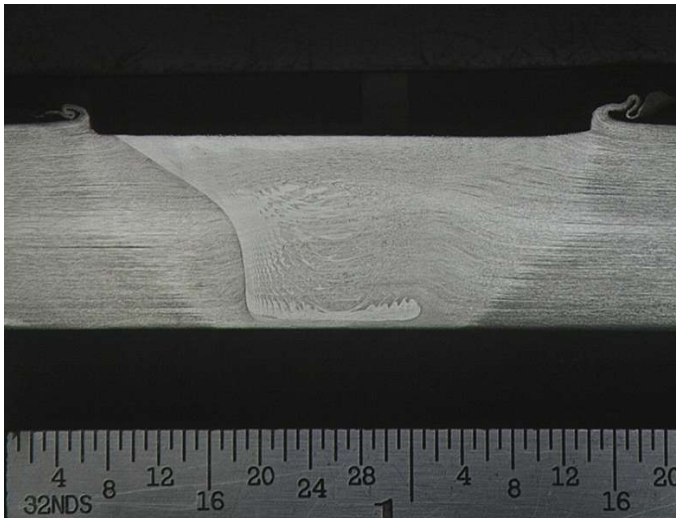


Figure 8. Polished and etched macro section from the slotted portion of weld PAR-17.

Microhardness indentations were taken along the mid-thickness of each sample (Figure 9). Readings (noted as '+' symbols) were collected in the center of the weld and across the HAZ on both the advancing and retreating sides. To ensure consistent spatial comparison, the innermost HAZ readings were positioned just inside the stir zone (SZ) boundary and progressed outward. This strategy permitted an evaluation of the local thermal cycle's impact on the material, specifically the overaging or softening that occurs just outside the mechanically refined zone. By anchoring the starting points within the SZ, corresponding HAZ data points were maintained at equal distances from the weld interface across all samples.

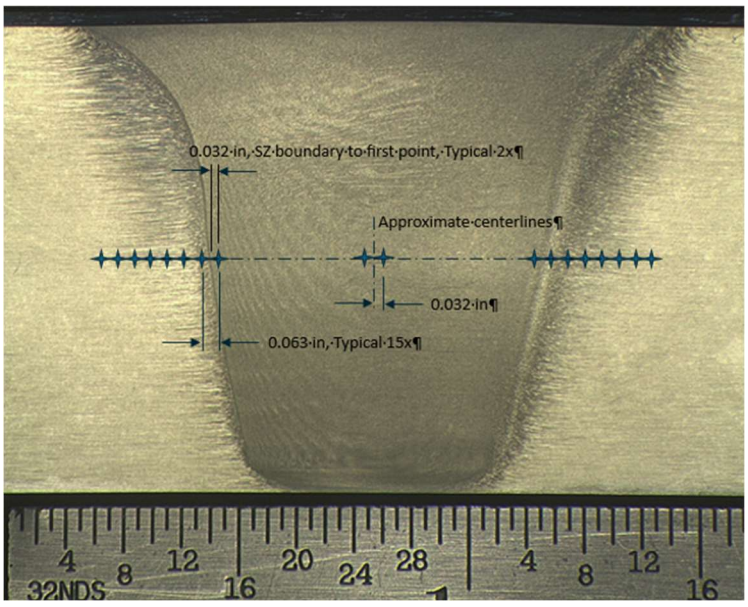


Figure 9. Microhardness test locations on a macro section of 25.4-mm 7075-T651 FSW.

When working with 7xxx-series aluminum, mechanical test results must account for the natural aging response of the workpiece. Because identical post-weld aging times are often impractical for all samples, a compensation method was employed based on the finding


DISTRIBUTION STATEMENT A. Approved for public release; distribution is unlimited. OPSEC#10639

that 7075 FSW specimens experience strength enhancement at a rate linear to a log-time scale [12]. To normalize these differences, microhardness readings from a single sample were taken at two different aging intervals to estimate the rate of hardness change. Most data points required a correction of only 1 Vickers hardness (Hv), with one sample requiring a 3 Hv adjustment. Using this method, all microhardness data were normalized to a baseline post-weld age of 1,344 hours.

Microhardness profiles for baseline welds PAR-12 and PAR-14 (Figure 10) illustrate the effects of varying flow stress and energy density setpoints under uniform boundary conditions (wide plates). While hardness values within 13 mm of the weld center were similar for both samples, PAR-14 exhibited a significantly lower minimum hardness in the HAZ. Additionally, the HAZ in PAR-14 was notably broader than in PAR-12. These results align with the lower flow stress setpoint used for PAR-14, which indicates a higher peak temperature and more extensive thermal softening.

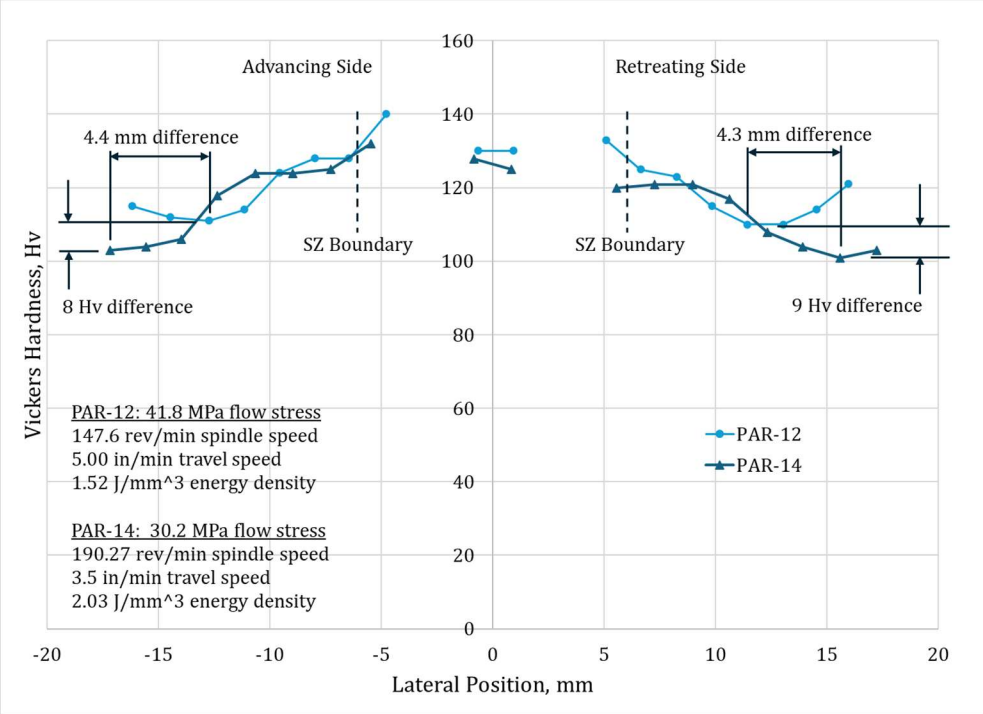


Figure 10. Microhardness measurements from welds PAR-12 and PAR-14, wide-plate boundary conditions welded with two different flow stress and weld pitch setpoints, 12.7-mm 7075-T651 FSW.

Microhardness results from "hot" welds made under flow stress control with weld pitch control, having setpoints of 30.2 MPa and 0.46 mm/rev, respectively, are shown in Figure 11. Despite varying boundary conditions and machine settings, maintained under forge load control, welds PAR-14 and PAR-21 exhibited nearly identical hardness values within 15 mm of the centerline. In contrast, PAR-17, made with the most restricted boundary condition, showed significantly lower hardness in this central region. Notably, the minimum hardness values for both PAR-21 and PAR-17 were nearly identical to each other, though both were slightly lower and broader than the baseline minimums for PAR-14.


DISTRIBUTION STATEMENT A. Approved for public release; distribution is unlimited. OPSEC#10639

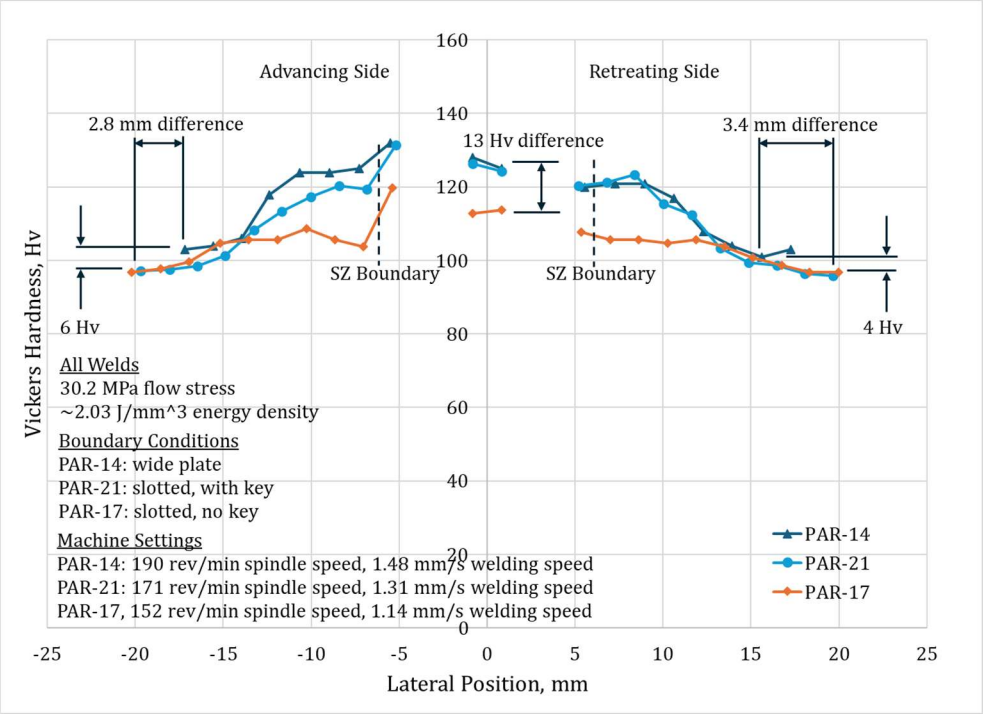


Figure 11. Microhardness measurements from welds PAR-14, PAR-17 and PAR-21, 30.2 MPa flow stress and 2.1 J/mm^3 energy density with different boundary conditions, 12.7-mm 7075-T651 FSW.

Figure 12 displays microhardness results for the “moderate” flow stress welds made with different boundary conditions. PAR-12 and PAR-22 were made at 42 MPa flow stress and 0.86 mm/rev weld pitch setpoints. Note that a weld with fully restricted boundaries (unfilled slots) was not feasible at this setpoint, as maintaining such a high flow stress would have required a spindle speed below the machine's minimum operational limit. Within 13 mm of the centerline, both welds exhibited similar hardness. However, in the HAZ, PAR-12 (baseline wide plate) maintained a significantly higher minimum hardness and a narrower HAZ than PAR-22. This indicates that the larger heat-sink of the wide plate better preserved HAZ properties compared to the keyed-slot configuration.


DISTRIBUTION STATEMENT A. Approved for public release; distribution is unlimited. OPSEC#10639

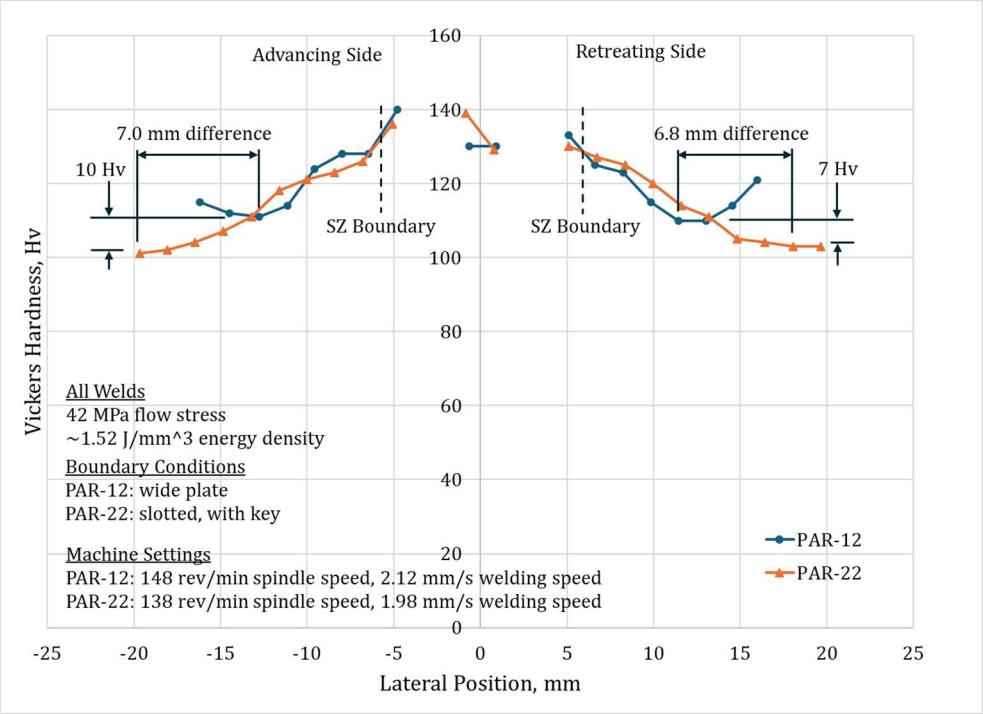


Figure 12. Microhardness measurements from welds PAR-12 and PAR-22, both made at 42 MPa flow stress and 1.52 J/mm^3 energy density, with different boundary conditions, 12.7-mm 7075-T651 FSW.

Figure 13 illustrates the relationship between minimum microhardness and energy density across all boundary conditions. For every specimen, the hardness minimum occurred within the HAZ. In the baseline, wide-plate welds, minimum hardness values were the highest overall and decreased as energy density increased. A similar downward trend was observed in the slotted plates with steel keys. In the most restricted boundary condition, slotted plates with no keys inserted, no change in minimum microhardness was observed at different energy densities. As conditions transitioned from wide plates to keyed slots and finally to empty slots, the minimum microhardness progressively declined until reaching an apparent floor of approximately 96 Hv.


DISTRIBUTION STATEMENT A. Approved for public release; distribution is unlimited. OPSEC#10639

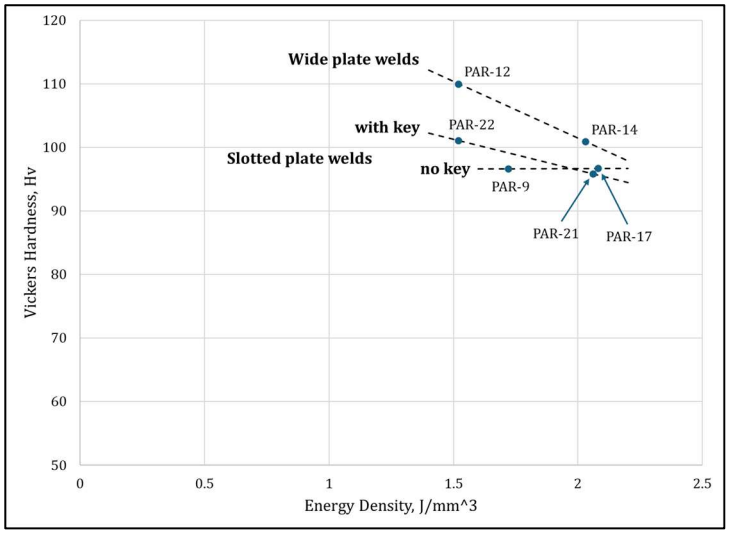


Figure 13. Minimum microhardness as a function of energy density, welds made with wide plates compared to those with restricted thermal boundary conditions.

## Discussion

Automated flow stress control successfully produced defect-free welds under severely restricted boundary conditions by modulating machine settings to maintain constant spindle torque, weld pitch, and plunge force. This adaptive transition preserved both surface quality and volumetric integrity despite the changing thermal sink. However, as shown in Figure 13, the mechanical properties remained sensitive to the boundary conditions. As the heat sink became more restricted, the minimum microhardness declined until reaching a plateau at approximately 96 Hv.

While this 96 Hv plateau represented the lower-bound mechanical state for the parameters tested, it likely reflects a regime of maximum precipitate overaging rather than full dissolution. Because the thermal cycles in this study may not have fully solutionized the HAZ, higher heat inputs or more prolonged thermal exposure could potentially lead to further precipitate dissolution and even greater softening upon slow cooling. Thus, while 96 Hv serves as a practical baseline for the adaptive control settings tested, further research is required to determine the absolute metallurgical floor for 7075-T651 under extreme thermal restriction.

This observed softening is a hallmark of 7075 aluminum, which exhibits high quench sensitivity where the primary driver of mechanical degradation is the time spent within the critical temperature range of 350°C to 250°C [12-15]. Prior studies have demonstrated a hardness-minimum plateau at low cooling rates where maximum precipitate coarsening occurs. In this regime, further reductions in the cooling rate do not significantly alter the resulting hardness [16]. These principles explain why microhardness was influenced by the reduced cooling rates inherent to restricted boundary conditions and why a consistent hardness floor was eventually observed.

These observations suggest that uniform tensile strength cannot be maintained in regions of restricted boundary conditions due to the inherent influence of reduced cooling rates.


DISTRIBUTION STATEMENT A. Approved for public release; distribution is unlimited. OPSEC#10639

Particularly for quench-sensitive alloys, the most effective welding procedure may only be able to guarantee volumetric soundness, achieved through adaptive control of flow stress or temperature, and a minimum plateau tensile strength in the most thermally restricted areas. Consequently, the traditional approach of qualifying fixed machine settings based on test plates with constant boundary conditions is not justified for joints with complex structural geometries.

In applications requiring high transverse strength despite restricted boundaries, external cooling (such as high-velocity compressed air or fluids) could counteract the reduced cooling rate, though this would likely only be effective in thinner workpieces where through-thickness thermal gradients are minimal. Alternatively, the flow stress control algorithm could be modified to allow weld pitch to increase in restricted regions, up to a specific threshold, to minimize the time spent above 250°C. To prevent the formation of wormhole defects, this maximum pitch would likely be a function of the specific welding tool design. Such a hybrid algorithm has been developed and remains a subject for future validation.

## Conclusions

This work resulted in the development of an adaptive algorithm that modulates spindle speed, welding speed, and plunge force to prevent volumetric defects and other quality demerits in regions of varying thermal boundary conditions. Preliminary, manual testing demonstrated that maintaining constant spindle torque, acting as a proxy for flow stress, preserved weld quality even under extreme thermal restriction. Subsequent automated implementation on a PAR Systems machine demonstrated the system's ability to modulate these parameters in real time, ensuring joint integrity without operator intervention.

While prior research indicates that transverse tensile strength is closely related to energy density, this study demonstrates that maintaining constant energy density is insufficient for preserving mechanical strength in regions of restricted boundary conditions. The reduced cooling rate inherent to these thermal barriers leads to additional microstructural coarsening in the HAZ. This localized softening can be mitigated by applying active cooling or by modifying the adaptive control algorithm to automatically increase weld pitch in restricted regions, thereby minimizing the time spent at critical overaging temperatures.

## Acknowledgements

The authors gratefully acknowledge the efforts of PAR Systems for implementing torque and weld pitch controls on their welding system and for supporting the welding experiments. The work of Ryan Tedjasukmana, Ryan Schuette, Daniel Langan and Jim Freeman is greatly appreciated.

This work was conducted under the program "Machine Learning for Advanced Lightweight Vehicle Structures" as part of a collaborative agreement between Concurrent Technologies Corporation and the National Center for Manufacturing Sciences, sponsored by the U.S. Department of Defense under Cooperative Agreement Award No. HP003424-2-0001. Special thanks to Mr. Michael Pollock of CTC and Mr. Martin McDonnell of the US Army DEVCOM GVSC for their support.


DISTRIBUTION STATEMENT A. Approved for public release; distribution is unlimited. OPSEC#10639

## References


1. Cederqvist, L., Bolsmjo, G. and Sorensen, C.D., "Adaptive control of novel welding process to seal canisters containing Sweden's nuclear waste using PID algorithms," Int'l. Conf. on Flex. Auto. and Intelligent Mfg., FAIM, Skovde, Sweden, 2008.
2. Fehrenbacher, A., Pfefferkorn, F.E., Zinn, M.R., Ferrier, N.J. and Duffie, N.A., "Closed-loop control of temperature in friction stir welding," 7th International Symposium on Friction Stir Welding, The Welding Institute, Cambridge, UK 20–22 May, 2008, Awaji Island, Japan.
3. Fehrenbacher, A., Duffie, N.A., Ferrier, N.J., Zinn, M.R. and Pfefferkorn, F.E., "Temperature measurement and closed-loop control in friction stir welding," 8th International Symposium on Friction Stir Welding, The Welding Institute, Cambridge, UK 18–20 May 2010, Timmendorfer Strand, Germany.
4. Mayfield, D.W. and Sorensen, C.D., "An improved temperature control algorithm for friction stir processing," 8th International Symposium on Friction Stir Welding, The Welding Institute, Cambridge, UK 18–20 May 2010, Timmendorfer Strand, Germany.
5. Cederqvist, L., Reynolds, A.P., Sorensen, C.D. and Garpinger, O., "Reliable FSW of copper canisters using improved process and regulator controlling power input and tool temperature," 8th International Symposium on Friction Stir Welding, 18–20 May 2010, Timmendorfer Strand, Germany.
6. Ross, K., "Investigation and implementation of a robust temperature control algorithm for friction stir welding," MS Thesis, Department of Mechanical Engineering, Brigham Young University, April 2012.
7. Colligan, K. and Hunt, J., "Effects of average flow stress and energy density in friction stir welded aluminum," International Friction Welding Conference 2026, The Welding Institute, Cambridge, UK, Cambridge, UK, 19–21 May, 2026.
8. Colligan, K., "Analysis of data from friction stir welds in aluminum," Presented at the Joint International Symposium on Friction Stir Welding and Processing, The Welding Institute, Cambridge, UK, Luneburg, Germany, 28–30 September 2022.
9. Colligan, K., "Analysis of torque data from friction stir welds in aluminum alloys," Friction Stir Welding and Processing XII, TMS (the Minerals, Metals and Materials Society), pp. 75–85, 2023.
10. Colligan, K., "Unit-area analysis of friction stir welding data," Presented at the 13th International Symposium on Friction Stir Welding and Processing, The Welding Institute, Cambridge, UK, Kyoto, Japan, 21–23 May, 2024.
11. Colligan, K., "Analysis of FSW macro-sections in aluminum relative to unit-area analysis," Friction Stir Welding and Processing XIII, TMS (the Minerals, Metals and Materials Society), pp. 215–232, 2025.
12. Fuller, C.B., Mahoney, M.W., Calabrese, M. and Micona, L., "Evolution of microstructure and mechanical properties in naturally aged 7050 and 7075 Al friction stir welds," Materials Science and Engineering A, vol. 527, pp. 2233–2240, 2010.
13. Nelson, T.W., Steel, R.J. and Arbegast, W.J., "*In situ* thermal studies and post-weld mechanical properties of friction stir welds in age hardenable Al alloys," Science and Technology of Welding and Joining, Vol. 8, No. 4, 2003.



DISTRIBUTION STATEMENT A. Approved for public release; distribution is unlimited. OPSEC#10639

14. Mahoney, M.W., Rhodes, C.G., Flintoff, J.G., Spurling, R.A. and Bingel, W.H., "Properties of friction stir welded 7075-T651 aluminum," Met. Trans. A, Vol. 29A, pp. 1955–1964, July 1998.
15. Su, J.Q., Nelson, T.W., Mishra, R. and Mahoney, M., "Microstructural investigation of friction stir welded 7050-T651 aluminum, Acta Materialia, vol. 51, pp. 713–729, 2003.
16. Saberi, L., Alfred, S.O. and Amiri, M., "Effects of quenching on corrosion and hardness of aluminum alloy 7075-T6," Energies, 15, 8391, 2022.


DISTRIBUTION STATEMENT A. Approved for public release; distribution is unlimited. OPSEC#10639